Fluctuation scaling in the visual cortex at threshold

José M. Medina* and José A. Díaz
Departamento de Óptica, Facultad de Ciencias, Universidad de Granada, Edificio Mecenas, 18071, Granada, Spain
(Received 1 November 2015; revised manuscript received 7 March 2016; published 6 May 2016)

Fluctuation scaling relates trial-to-trial variability to the average response by a power function in many physical processes. Here we address whether fluctuation scaling holds in sensory psychophysics and its functional role in visual processing. We report experimental evidence of fluctuation scaling in human color vision and form perception at threshold. Subjects detected thresholds in a psychophysical masking experiment that is considered a standard reference for studying suppression between neurons in the visual cortex. For all subjects, the analysis of threshold variability that results from the masking task indicates that fluctuation scaling is a global property that modulates detection thresholds with a scaling exponent that departs from 2, $\beta = 2.48 \pm 0.07$. We also examine a generalized version of fluctuation scaling between the sample kurtosis K and the sample skewness S of threshold distributions. We find that K and S are related and follow a unique quadratic form $K = (1.19 \pm 0.04)S^2 + (2.68 \pm 0.06)$ that departs from the expected 4/3 power function regime. A random multiplicative process with weak additive noise is proposed based on a Langevin-type equation. The multiplicative process provides a unifying description of fluctuation scaling and the quadratic S-K relation and is related to on-off intermittency in sensory perception. Our findings provide an insight into how the human visual system interacts with the external environment. The theoretical methods open perspectives for investigating fluctuation scaling and intermittency effects in a wide variety of natural, economic, and cognitive phenomena.

DOI: 10.1103/PhysRevE.93.052403

I. INTRODUCTION

One of the most fundamental aspects of human perception and action is the existence of irregular trial-to-trial variability under repeated tasks. The study of fluctuations in perception has been traditionally oversimplified by assuming independent measurements over time. However, a large body of experimental data has pointed out that trial-to-trial variability could reflect nontrivial correlations in both neural activity and human behavior [1–6]. An important empirical relationship concerns fluctuation scaling [7,8] (also known as "Taylor's law" in ecology) [7,9]. Fluctuation scaling states that the size of fluctuations as measured by the sample variance (σ^2) and the sample mean (μ) can be fitted approximately by a power function with a scaling exponent $\beta > 0$:

$$\sigma^2 = \alpha \mu^{\beta}, \tag{1}$$

where α is a coefficient ($\alpha > 0$) [7,9,10]. Fluctuation scaling is a general tendency rather than a physical law [7]. Fluctuation scaling is often considered an emergent collective property and has been widely reported in complex dynamical systems although departures from the power function have been also reported in different fields [7]. Different models of fluctuation scaling have been proposed in ecology, physics, biology, etc. [7,9–17]. In particular, fluctuation scaling has an important impact on human activity [7,12,18,19] and in the nervous system at different levels of analysis; from variability of spike trains at a microscopic level [20–25] to variability in human psychophysics at a macroscopic level [26–30]. Nonetheless, although psychophysical studies have confirmed an increasing trend between σ^2 and μ, they were not oriented to obtain a reliable estimation of the exponent β over at least two orders of magnitude [7,31,32] and, hence, they lack statistical support [32].

In this paper we describe and show results of a simple experiment that demonstrates fluctuation scaling in human color vision at threshold. Here we examine the subject's response variability during a standard psychophysical task that consists of detecting thresholds for spatial gratings presented on a computer screen [33,34]. We have used a statistical approach where trial-to-trial threshold variability is characterized by the moments of the probability density function (PDF). We have measured the mean μ and the variance σ^2 of threshold distributions over a broad range of experimental conditions. Understanding the statistical properties of PDFs is an important issue in visual neuroscience and psychophysics because thresholds mediate visual perception and action in everyday actions and for modeling PDFs. Together with the mean μ and the variance σ^2, we further investigate the shape of threshold distributions by examining higher-order statistics, namely, the sample skewness (S) and the sample kurtosis (K). The skewness S provides a measure of the asymmetry of the PDF, whereas the kurtosis K provides a measure of the peakedness of the PDF and heaviness of its tails [35]. $S = 0$ indicates a perfect symmetric Gaussian distribution and deviations to the right and to left of the mean value are represented by $S > 0$ and $S < 0$, respectively. The kurtosis of a Gaussian distribution has a value of 3. A distribution with $K > 3$ indicates a higher peak and heavy tails, otherwise for $K < 3$ the distribution flattens. By representing K as a function of S, i.e., the S-K plane, non-Gaussian processes often follow a parabolic shape near the Gaussian point $(S, K) = (0, 3)$. This parabolic relationship is not trivial and indicates a general relation in the analysis of PDFs in a variety of fields such as in plasma physics [36–43], weather and climate [38,44], contaminant concentration fluctuations in the atmosphere [45–49], laser chaotic dynamics [50], neural spike counts [51], etc. Its origin has been investigated by using empirical

*jmedinaru@cofis.es

models of PDFs [36,51–58], as well as physical models [38,43,45,49,59–63]. However, there are also non-Gaussian processes that exhibit a second regime in the S-K plane by showing extreme events. These extreme events occupy the tails of PDFs and often produce very large S and K values that lie above the parabolic region. They are better described by a power function with a scaling exponent γ near to 4/3 [56]. These processes are typically observed in earthquakes, financial data, etc. [56].

We will demonstrate that fluctuation scaling is quite robust and governs variability of threshold responses for a wide range of experimental conditions in human color vision. Furthermore, we will show that K and S of threshold histograms vary by following a U-shaped pattern. A unique quadratic relationship is found in the same way as in many dynamical processes suggesting perhaps a unifying description. The results show how fluctuation scaling modulates the dynamical behavior of visual signal detection under masking and are important to better understand the macroscopic effects of brain activity in sensory perception.

The paper is organized as follows. In Sec. II we explain theoretically that the 4/3 regime in the S-K plane is a generalized version of fluctuation scaling. Section III describes the psychophysical methods and procedure employed. In Sec. IV we report the experimental results and explain that contrast detection thresholds in visual masking are the result of intermittency of a special kind. We present a stochastic process driven by multiplicative and weak additive noise based on a Langevin-type model. The Langevin model provides a unified description of the experimental data. We will explain why our threshold data deviate from the 4/3 power function regime and follow a characteristic quadratic relation in the S-K plane. We also discuss the relevance of our findings in comparison with previous physical models of the quadratic S-K relation. Concluding remarks are summarized in Sec. V.

II. THEORETICAL BACKGROUND

Many theoretical models have explained fluctuation scaling in a wide range of ecological, biological, and physical phenomena, etc. [7,9–17], but the existence of a universal mechanism remains elusive. Simulations based on a class of multiplicative growth processes have concluded that a finite number of observations can lead to fluctuation scaling. Two different regimes have been identified in the temporal evolution of the scaling exponent β in Eq. (1). In the former regime, limited sampling over small time windows lead to abrupt changes in β. These changes may differ from 2 and are associated with transitions in the external environment. In the second regime, limited sampling over very long time windows lead to a scaling exponent β that moves close to 2 regardless of the nature of the underlying dynamical process. In the same regime, a generalized version of fluctuation scaling was derived based on the sample moments of PDFs [16]. The 4/3 power function in the S-K plane [56,58] is indeed a true manifestation of a generalized version of fluctuation scaling under the conditions stated in [16]. To explain this issue theoretically, we will use the sample moments of a generic PDF containing N data points. The first moment m_1 is the sample mean μ. The subsequent moments can be centered around the mean value as follows [35]: $m_r = (1/N)\sum_{i=1}^{N}(x_i - \mu)^r$, where x_i are the experimental data. In our case r runs up to the fourth sample moment $r = 2,3,4$. The generalized version of fluctuation scaling states that the third and fourth moments should converge to a power function at very long times with a scaling exponent equal to 4/3 [16], $m_4 = \varphi m_3^{4/3}$, where φ is a coefficient. By definition, the skewness S and the kurtosis K are the standardized third and fourth sample moments, respectively [35], and consequently $m_3 = S_0 m_2^{3/2}$ and $m_4 = K_0 m_2^2$. S_0 and K_0 refer to the unbiased formulas [64]. By substituting m_4 and m_3 into the above generalized version of fluctuation scaling it follows $K_0 = \varphi S_0^{4/3}$. This approach provides an alternative explanation to current theories of the 4/3 power function in the S-K plane [56,58] and is not specific for K and S but general under the assumptions of the theory stated in [16]. The generalized version of fluctuation scaling for the jth and the ith sample moments ($i < j$) can be written as $m_j = \varphi_{j,i} m_i^b$ asymptotically in time [16]. The scaling exponent $b = j/i$ recovers the conventional version of fluctuation scaling with $j = 2$ and $i = 1$ [16]. Our main purpose is to investigate whether temporal fluctuation scaling (i.e., the statistical properties are calculated over time) [7] holds in human color vision at threshold between σ^2 versus μ, as well as between K versus S over a broad range of experimental masking conditions.

III. EXPERIMENTAL METHODS

A. Visual task

Here we focus on a task particularly concerned with orientation-tuned mechanisms. Orientation processing is a fundamental feature of most cortical visual neurons [65]. Contrast detection thresholds were measured when using test gratings overlaid by masking gratings of similar shape and frequency but orthogonally oriented (i.e., "plaids") [66,67]. This cross-orientation masking task is a canonical paradigm that simulates pattern detection in complex visual scenes. In cross-orientation masking, mask stimuli interfere with the test stimulus and produce a threshold elevation of the test stimulus at high mask levels [66–69]. Furthermore, cross-orientation masking in humans has an analogy from the behavior of cross-orientation suppression in cortical visual neurons. In cross-orientation suppression, the response of a single neuron that is tuned to a preferred oriented grating is reduced by the superimposition of an orthogonally oriented grating [70,71]. Cross-orientation suppression has become a reference paradigm in visual neuroscience for understanding neural computation in the visual cortex and involves subcortical and cortical visual neurons [72,73].

B. Stimuli

We have reanalyzed data sets from two different psychophysical studies that employed similar experimental devices and protocols [67,69]. Preliminary results have been reported elsewhere [74]. Stimuli were displayed on a calibrated computer-controlled cathode-ray tube monitor using a specialized graphics card for stimulus generation. Experiments were created by using the Psychophysics Toolbox [75,76].

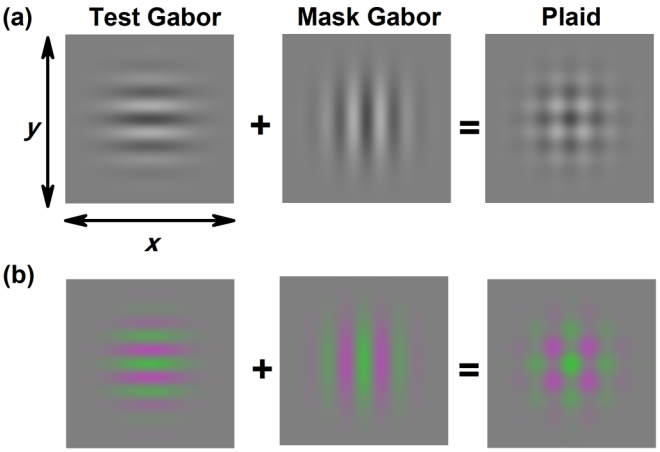

FIG. 1. (a) Example of a horizontally oriented achromatic test Gabor patch, orthogonal mask, and both superimposed as a plaid at high contrasts. In the example the spatial frequency is 0.375 cpd. (b) Red-green stimuli at isoluminance. The luminance level remains constant but producing a chromatic signal. The same spatial frequency follows as in (a).

Test stimuli were horizontally oriented Gabor patches. Gabor patches can be generated by the multiplication of a two-dimensional spatial sine wave as the carrier and a Gaussian profile as the envelope [77]. Test and mask Gabor patches were coincident in spatial and temporal frequencies and phases, where the mask stimuli is a vertical Gabor patch, in order to be orthogonally oriented to the horizontal test Gabor patch. Plaids were also contrast modulated by using a temporal sinusoidal waveform in a temporal Gaussian envelope. A schematic representation of a test and a mask Gabor patches and the resulting plaid stimuli are shown in Figs. 1(a) and 1(b).

Both test and mask contrast values were scaled by using the conventional Michelson contrast $(I_{\max} - I_{\min})/(I_{\max} + I_{\min})$, in which $I_{\max}$ and $I_{\min}$ indicate the maximum and minimum luminance amplitude in the visual pattern, respectively. Stimuli were achromatic (i.e., grayscale) [Fig. 1(a)] and red-green isoluminant, which eliminates any transient luminance changes [Fig. 1(b)]. This affords us the possibility to examine whether different visual mechanisms contribute to fluctuation scaling. In current color vision models, M_1 (long-), and M_2 (middle-), and M_3 (short-) wavelength-sensitive photoreceptor signals are reorganized into three separate post-receptoral mechanisms or orthogonal cone axis: a luminance $(M_1 + M_2)$ axis and a red-green $(M_1 - M_2)$ and a blue-yellow $[M_3 - (M_1 + M_2)]$ cone opponent axis [67,78]. Cone opponency is a fundamental characteristic of color coding in human vision. Here we have used both achromatic and red-green stimuli. Achromatic stimuli are mediated by the luminance system, whereas red-green isoluminant stimuli isolate the activity in the red-green color vision system [67,78,79]. For red-green isoluminant stimuli, test and mask contrast values were initially represented in the cone contrast space [79]. This is a three-dimensional orthogonal space often used in color vision research by using the cone excitation values. Cone excitation values of visual stimuli are computed by using the quantal catch rates of absorption for the M_1, M_2, and M_3 signals, respectively. The cone fundamentals of Smith and Pokorny were used [80]. The

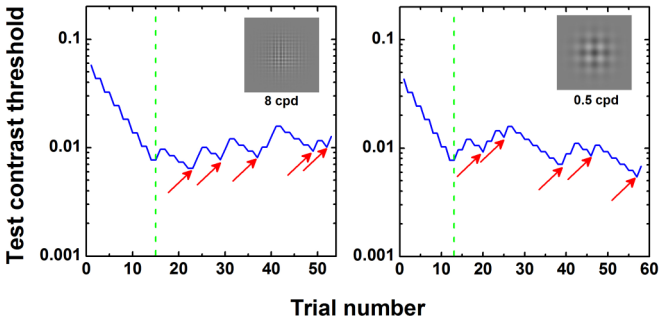

FIG. 2. Typical examples of a 2AFC staircase procedure at different stimulus configurations. Semilogarithmic plot ($\log_{10}$) of the stimulus contrast threshold as a function of the trial number. The vertical dashed lines indicate the first reversal point. Arrows indicate subsequent reversal points.

coordinates in the cone contrast space are defined as the cone excitation signal difference between the test and the reference relative to the reference stimulus or the Weber fractions $[(\Delta M_1/M_1),(\Delta M_2/M_2),(\Delta M_3/M_3)]$. The vector length in the cone contrast space defines the chromatic contrast of stimuli $[(\Delta M_1/M_1)^2 + (\Delta M_2/M_2)^2 + (\Delta M_3/M_3)^2]^{1/2}$. Then, chromatic contrast values are transformed to the Michelson contrast dividing by a scaling factor of $\sqrt{3}$ [67,79]. Stimuli were observed in binocular or monocular vision in fovea and by using natural pupils [67,69].

C. Procedure

A conventional temporal two-alternative forced-choice (2AFC) staircase procedure provided an estimation of the subject's threshold response. 2AFC staircase methods are standard in human psychophysics and have been used extensively in a large number of experimental studies [33,34,81]. They minimize the influence of a subject's response bias and produce a high level of performance for threshold estimation [33,34,81]. Two time intervals contain a vertically oriented mask Gabor at a fixed contrast value or the mask contrast C. In one of the two temporal intervals, a horizontally oriented test Gabor with the same spatiotemporal configuration was superimposed with a lower test contrast. The stimulus variable is the contrast of the test Gabor or the test contrast and the subject is forced to indicate which interval contained the test Gabor. A classical two-down–one-up rule was implemented over successive trials. If the subject responds correctly twice, the test contrast level steps down by a fixed discrete value Δ^-, otherwise an incorrect response steps up the test contrast level by a fixed discrete value Δ^+ [67,69,81]. Examples of up-down staircase sessions as a function of the trial number are represented in Fig. 2 for different stimulus configurations.

The starting test contrast value was chosen above the threshold level. In a 2AFC staircase procedure a response reversal is a transition point of the subject's response and can be defined when the subject has responded incorrectly after at least two consecutive correct responses [33,34,81]. Response reversals indicate the most favorable experimental conditions to estimate the threshold and are the basis to calculate the statistical properties of threshold distributions. The first reversal was used to reach the threshold level and was

always discarded from subsequent analyses (vertical dashed lines in Fig. 2) [33,81]. Each experimental configuration was established by selecting a specific spatial and temporal frequency, viewing condition (binocular or monocular), and type of stimuli (achromatic or red-green isoluminant). Cross-orientation masking was examined over a wide range of suprathreshold mask contrasts C from 0.1% to 30% [67,69]. For each stimulus condition, the number of total trials in a 2AFC staircase session varied between 30 and 70 trials [67,69,81]. The number of staircase sessions varied between 4 and 8 sessions [67,69,81].

D. Data analysis

The mean threshold μ was calculated by using the common method of taking the sample arithmetic mean of the test stimulus contrast over a number of reversals over time [33,34,81]. We used the last five reversal values of each staircase session [67,69]. The percentage of correct performance of the visual task was near 80% [33,34,81]. The threshold variability was calculated as the displacement of the test contrast at the reversal points x_i with respect to their mean μ by using the sample variance $\sigma^2 = (1/N-1)\sum_{i=1}^{N}(x_i-\mu)^2$, where N is the total number of reversals in the time series. Both the sample skewness S_0 and kurtosis K_0 were calculated at the reversals as well and were corrected for bias [64]:

$$\begin{aligned} S_1 &= \frac{[N(N-1)]^{1/2}}{N-2}S_0, \\ K_1 &= \frac{N-1}{(N-2)(N-3)}[(N+1)K_0 - 3(N-1)] + 3. \end{aligned} \tag{2}$$

We fitted σ^2 as a function of μ by using a power function. A linear least-squares regression was performed in a log-log plot [7,31] by minimizing the Chi-square value [82]. The goodness-of-fit was evaluated by using the coefficient of regression R-square or R^2.

E. A power function model in the skewness-kurtosis plane

It is well known that the kurtosis K and the skewness S are related and have a lower bound for any PDF with $\sigma \neq 0$, $K \geqslant S^2 + 1$ [52,53], and for the class of unimodal PDFs, $K \geqslant S^2 + 189/125$ [54]. For a large body of experimental data from many different physical situations, the relation between K and S is a well defined power function with an exponent of 2 [37–43,45–50]:

$$K = AS^2 + B, \tag{3}$$

where A and B are the amplitude and the offset, respectively ($A > 0, B > 0$). Both A and B have different values in the literature that depend on the context [37–43,45–50]. We have compared the quadratic form in Eq. (3) against a simplified version with one parameter ($A = B$), $K = A(S^2 + 1)$ [48]. This model is an extended version of the statistical limit $K = S^2 + 1$ [52,53]. We have also compared Eq. (3) against a generic parabola with three parameters $K = AS^2 + DS + B$, where D is a new coefficient ($D > 0$) [43,44,55,63]. The main difference between Eq. (3) and the parabola model is that Eq. (3) implicitly assumes the existence of symmetry in the human visual system. That is, K must be invariant with respect to the sign inversion of S and consequently $D = 0$ in Eq. (3) [43,55,56,62]. We further compared Eq. (3) against a symmetric power function with the scaling exponent γ as a free parameter $K = A|S - S_R|^\gamma + B$, where S_R is the center. The symmetric power function model has four parameters and is a generalized version of the above symmetry which is now located around the center S_R. In all models, a nonlinear least-squares regression was also performed between unbiased K_1 and S_1 values by minimizing the Chi-square value. The Chi-square value was normalized to the different degrees of freedom $\bar{\chi}^2$. The parameters values were obtained by using the Levenberg-Marquardt algorithm [82].

F. Subjects

Data sets come from six healthy subjects (labeled as P1, P2, P3, P4, P5, and P6). All the subjects had normal color vision and visual acuity according to standard clinical tests. All subjects were also experienced and familiar with visual tasks. Subjects P1, P2, and P3 participated in a cross-orientation masking experiment where the spatiotemporal configuration of Gabor stimuli were selected at the spatial frequencies of 0.375, 0.75, and 1.5 cpd (cycles per degree) and at the temporal frequencies of 2, 4, and 8 Hz [67]. Subjects P4, P5, and P6 participated in a cross-orientation masking experiment where Gabor stimuli were configured at a different range: 0.5 cpd, 8 Hz and 8 cpd, 1 Hz at different adapting conditions [69].

IV. RESULTS AND DISCUSSION

A. Test threshold versus mask contrast

Figure 3 shows an example of the test threshold μ as a function of the mask contrast C, i.e., the conventional threshold vs contrast (TvC) curve in spatial vision [66–69,83]. Error bars indicate one standard deviation σ. This particular example corresponds to the TvC function of one subject (P2) in binocular vision and for achromatic Gabor stimuli at 0.375 cpd, 8 Hz sampled at ten different mask contrasts [67].

The shape of the TvC function is nonlinear and has been confirmed extensively in many psychophysical experiments [66–69,83]. At high mask contrast values the vertical mask Gabor interferes with the horizontal test Gabor and a threshold elevation is often produced (Fig. 3). The threshold elevation depends on the spatial and temporal frequencies of achromatic Gabor gratings and viewing conditions and is stronger when using chromatic stimuli [67–69,83]. However, the mask stimulus could enhance the test contrast detection threshold at intermediate mask contrasts C. This facilitation effect is lower than the test contrast detection threshold in the absence of mask stimuli in some stimulus configurations (horizontal dashed line in Fig. 3). This is often a small but ubiquitous effect that has been reported elsewhere in sensory psychophysics (also known as the dipper effect or negative masking) [66–69,84]. This issue will be discussed further below.

B. Fluctuation scaling in cross-orientation masking

Figure 4(a) presents the sample variance σ^2 as a function of the sample mean value μ combined from all six subjects together. Data points indicate 392 stimulus conditions that

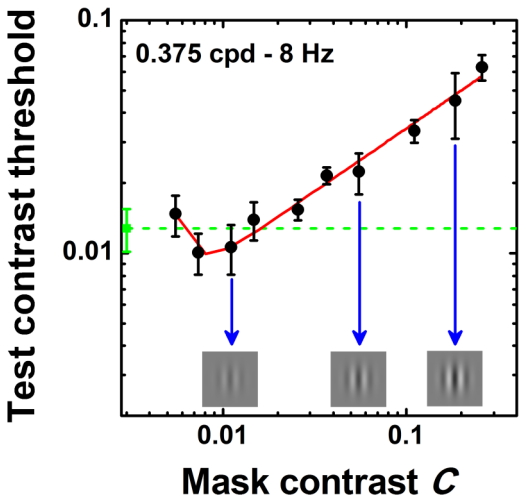

FIG. 3. Example of cross-orientation masking in human vision. Double logarithmic plot ($\log_{10}$) of the test contrast detection threshold versus mask contrast C for achromatic Gabor gratings at 0.375 cpd, 8 Hz. Solid circles indicate the mean threshold value in binocular vision from one subject (P2). The solid square at the left and the corresponding horizontal dashed line indicate the threshold level that denotes no effect of the mask on the test Gabor grating. Points above and below the dashed line indicate threshold elevation and facilitation, respectively. Error bars are one standard deviation. The solid line indicates the best fit to the equation $y = (6 \times 10^{-14}/C^{4.9}) + 0.12C^{0.5}$ (see Sec. IV D). Vertical arrows show a schematic representation of the vertical mask Gabor at different mask contrasts C.

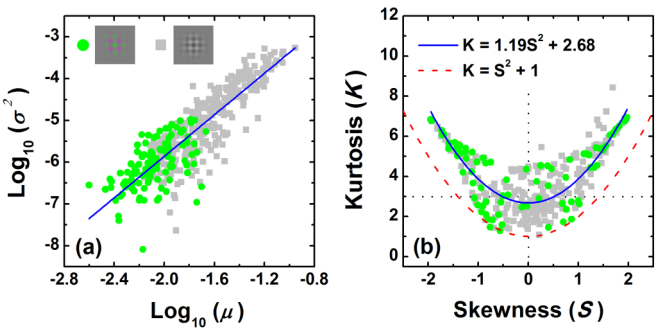

FIG. 4. (a) Double logarithmic plot ($\log_{10}$) of the sample variance σ^2 as a function of the sample mean μ from all subjects together. Solid line indicates a linear fit $\log_{10}(\sigma^2) = \log_{10}(\alpha) + \beta\log_{10}(\mu)$, where α is a coefficient and β is the slope, $\beta = 2.48 \pm 0.07$, where the error is the standard error. (b) Linear plot of the kurtosis K_1 versus skewness S_1 from all subjects together. The solid line indicates the best fit to a power function with an exponent of 2, $K_1 = (1.19 \pm 0.04)S_1^2 + (2.68 \pm 0.06)$, where errors are standard errors. The dashed line indicates the statistical limit $K = S^2 + 1$ [52,53]. Vertical and horizontal dotted lines indicate $S = 0$ and $K = 3$, respectively. The intersection of dotted lines corresponds to the Gaussian point. In (a) and (b) data points represent a total of 392 and 318 stimulus conditions, respectively, that result from the combination of all spatial and temporal frequencies, mask contrast values, viewing conditions (binocular and monocular), type of stimuli (achromatic and red-green isoluminant), and masking effects (threshold elevation and facilitation). Solid circles and squares represent the values for red-green isoluminant and achromatic stimuli, respectively.

result from the combination of different spatial and temporal frequencies, viewing conditions (binocular and monocular), and type of stimuli (achromatic and red-green isoluminant) [67,69].

Data points roughly span two orders of magnitude. The mean value μ ranges from 0.0025 to 0.11 and the variance σ^2 from 8×10^{-9} to 5×10^{-4}. Fluctuation scaling in Eq. (1) is revealed as a linear relationship with the scaling exponent $\beta = 2.48$ and with 95% confidence intervals (2.33,2.62). Remarkably, red-green isoluminant σ^2 values are clustered at low μ values and extend the linear regime of fluctuation scaling. This suggests a common mechanism that produces long-term correlations averaged across subjects and regardless of the type of stimuli (achromatic and red-green isoluminant) and masking effect (threshold elevation and facilitation) (Fig. 3). There is some broadening in the experimental data [7] and the linear fit explains around 74.5% of total variability of data points. Similar results are obtained when the trial number orders the reversal points (Fig. 2) by using the mean square successive difference [74,85].

C. The skewness-kurtosis plane

Figure 4(b) represents in a linear plot the unbiased sample kurtosis K_1 as a function of the unbiased sample skewness S_1 for 318 stimulus conditions. We found that some stimulus configurations produce K and S values below the statistical limit $K = S^2 + 1$ [52,53]. This was due to short samples where the number of reversal points was small in those particular configurations. These data points were filtered out in subsequent analysis. The results confirm the existence of non-Gaussian statistics. Data points show higher and lower K values than the Gaussian distribution ($K = 3$) and both positive and negative S values as well. A U-shaped pattern is clearly observed averaged across observers, viewing and stimulus conditions, masking effects (threshold elevation and facilitation), and type of stimuli (achromatic and red-green isoluminant). Data points for red-green isoluminant stimuli are clustered around the borders, whereas those for achromatic stimuli cover the entire U-shaped pattern but they are mainly clustered at the center near the Gaussian point. There are no large deviations and K ranges from 1.07 to 8.43, whereas S ranges from -1.95 to 1.97. The quadratic relation in Eq. (3) has $\bar{\chi}^2 = 0.726$ and provides a reasonable good fit by explaining 69% of total variability ($R^2 = 0.69$), $K_1 = (1.19 \pm 0.04)S_1^2 + (2.68 \pm 0.06)$. Errors are standard errors. In comparison with other models, the one-parameter quadratic polynomial [48] $K_1 = A(S_1^2 + 1)$ does not improve the minimization of the $\bar{\chi}^2$ and can be discarded. Both the parabola $K_1 = AS_1^2 + DS_1 + B$ [43,44,55] and the symmetric power function model $K_1 = A|S_1 - S_R|^\gamma + B$ have similar values and $\bar{\chi}^2 = 0.722$ and $\bar{\chi}^2 = 0.724$, respectively. However, in both models the coefficients A and B were similar to those values obtained in Eq. (3) and the new added parameters were nearly zero, $(D = 0.08 \pm 0.05)$ and $(S_R = -0.03 \pm 0.02)$. Furthermore, the scaling exponent γ in the symmetric power function model does not converge to 4/3 [16] and was very near to 2 ($\gamma = 1.95 \pm 0.16$). Therefore, the justification of the parabola and the symmetric power function model with three

and four parameters, respectively, is difficult to maintain and both models can be discarded [43,55].

The A and B values of Eq. (3) in cross-orientation masking are similar to other variables in climate, plasma physics, etc. [36–39,41,42,44,46,47,49,50,61]. They are particularly close to data from a grid-turbulence laboratory plume experiment in atmospheric science [49]. We repeated the same analysis by excluding those masking conditions that produce threshold facilitation (Fig. 3). The coefficients A and B were similar and do not change the conclusions. This indicates that threshold facilitation in Fig. 3 is a tiny effect that does not produce very large S and K values in the experimental conditions analyzed. The masking effects that lead to threshold elevation largely dominate the U-shaped pattern in Fig. 4(b).

D. A random multiplicative process with additive noise

The sample mean, variance, skewness, and kurtosis in Fig. 4 were calculated by using the reversal points at local minima as shown in Fig. 2 [33,34,81]. In general, the subject's responses in a temporal 2AFC procedure alternate between two different phases. In Fig. 2, the first phase is a "laminar" or periodic regime where the test contrast threshold follows similar trajectories and increases or decreases as a function of the trial number. The second phase is a "turbulent" regime that corresponds to aperiodic transition points at local minima and separates the two types of trajectories (Fig. 2). This can lead to on-off intermittency [86–88] in the same way as different experimental paradigms [89,90]. We propose that on-off intermittency as measured by the reversal points plays a key role in human psychophysics by shaping the moments of threshold distributions. We investigate this issue by adapting a model proposed by Nakao [91] to cross-orientation masking. Here we focus on the reversal points at local minima. A similar treatment can be performed on the transition points at local maxima (Fig. 2). We propose that the reversals x_i as a function of the ith trial number (Fig. 2) are driven by multiplicative and additive noise. We have employed a discrete-time Langevin equation [91,92]:

$$x_{i+1} = \lambda_i x_i + \eta_i, \tag{4}$$

where λ_i and η_i are stochastic variables that represent a multiplicative and an additive noise term, respectively. Those λ_i values higher than unity ($\lambda_i > 1$) will amplify the magnitude of reversals where those below unity ($0 < \lambda_i \leqslant 1$) will diminish it. The additive noise term η_i is of special relevance because it prevents that the reversals x_{i+1} collapse to zero when λ_i tends to zero. The multiplicative and the additive noise are delta correlated $\langle \lambda_i, \lambda_j \rangle = F_\lambda \delta_{i,j}$ and $\langle \eta_k, \eta_l \rangle = F_\eta \delta_{k,l}$, respectively, and both are on average $\langle \lambda_i \rangle \propto F_\lambda$ and $\langle \eta_i \rangle \propto F_\eta$, respectively. The bracket $\langle \cdots \rangle$ indicates the time average over the reversals. F_λ and F_η are the diffusion coefficients of the multiplicative and the additive noise, respectively, and indicate the average strength of interactions [91,92]. We assume that both F_λ and F_η are state dependent. F_λ promotes the reversals to a minimum value and decreases as the mask contrast C increases [22,93], $F_\lambda = J_\lambda / C^\omega$, where J_λ and ω are a coefficient and the scaling exponent, respectively. However, the additive noise strength controls the masking effect and increases as the mask contrast increases, $F_\eta = J_\eta C^\varepsilon$, where J_η and ε are a coefficient and the corresponding scaling exponent, respectively. Taking the time average over the reversals in Eq. (4), the physical mechanism of the TvC functions is revealed. The mean test contrast detection threshold $\langle x_{i+1} \rangle$ as a function of the mask contrast C is the result of the interplay between the multiplicative and the additive noise terms:

$$\langle x_{i+1} \rangle = \frac{J_\lambda x_0}{C^\omega} + J_\eta C^\varepsilon. \tag{5}$$

For increasing the mask contrast C, the multiplicative noise strength drops to zero from a reference value x_0, while the additive noise strength increases and compensates the above multiplicative effect. The scaling exponents ω and ε control the multiplicative and the additive noise strength as a function of the mask contrast, respectively. The dipper effect of the TvC functions (Fig. 3) is the result of a balance when the strength of both noise terms is weak and is equivalent to a resonance-type effect [84]. In general, the dipper effect in cross-orientation masking is less pronounced (Fig. 3), except for achromatic stimuli at high spatial frequencies [66,68,69]. Figure 5(a) shows a numerical simulation of the time average $\langle \lambda_i \rangle = F_\lambda$ and $\langle \eta_i \rangle = F_\eta$ separately.

The shape of the TvC function can be modulated by assuming that J_η depends on the spatiotemporal configuration of Gabors and type of stimuli (achromatic and red-green isoluminant) processed by the different parallel visual pathways [78,94]. The product $J_\lambda x_0$ also depends on the viewing

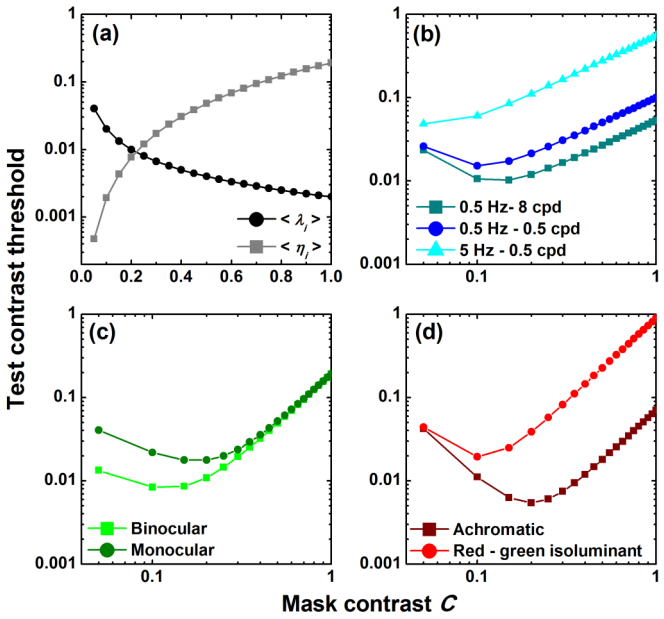

FIG. 5. (a) Semilogarithmic plot ($\log_{10}$) of the time average of the multiplicative $\langle \lambda_i \rangle$ and the additive noise term $\langle \eta_i \rangle$ of the Langevin model. The parameters are $x_0 = 0.1$, $\omega = 1$, $\varepsilon = 2$, $J_\lambda = 0.02$, $J_\eta = 0.18$. (b) Double logarithmic plot ($\log_{10}$) of the TvC functions for achromatic gratings for several values of the temporal and the spatial frequency: $x_0 = 0.032$, $\omega = 2$, $\varepsilon = 1$, $J_\lambda = 0.05$, $J_\eta = 0.053$ (squares), $J_\eta = 0.1$ (circles), $J_\eta = 0.55$ (triangles). (c) TvC functions for binocular and monocular vision: $x_0 = 0.032$ (binocular), $x_0 = 0.1$ (monocular), $\omega = 1$, $\varepsilon = 2$, $J_\lambda = 0.02$, $J_\eta = 0.19$. (d) TvC functions for achromatic and red-green isoluminant stimuli: $x_0 = 0.032$, $\omega = 2$, $\varepsilon = 2$, $J_\lambda = 0.07$, $J_\eta = 0.07$(achromatic), $J_\eta = 0.9$(red-green).

conditions (binocular and monocular). Figures 5(b), 5(c), and 5(d) show three representative numerical examples by using Eq. (5). Other examples follow in a similar way. In the first example in Fig. 5(b), the TvC function for achromatic stimuli has a spatiotemporal dependence, in which the threshold elevation due to the mask contrast increases as the temporal frequency increases and the spatial frequency decreases [66–69]. The second example illustrates a binocular summation effect at low mask contrast values [69,83] [Fig. 5(c)]. The contribution of the different retinocortical pathways [78,94] is captured in the third example in Fig. 5(d). Threshold elevation for red-green isoluminant stimuli is stronger at low spatial and temporal frequencies [67].

E. The effect of weak additive noise

The Langevin model in Eqs. (4) and (5) is one of the basic stochastic models that produce power laws at the right tail of PDFs in different contexts such as in econophysics [95–97], mental chronometry [98], etc. In Eq. (5) a weak additive noise strength is important when the amplitude of reversals is not very large (Fig. 2) and guarantee the existence of a stationary PDF with power-law tails under boundary conditions [91]. Time series in 2AFC processes, as the examples shown in Fig. 2, are bounded ($0 < x_{i+1} < 1$). There is a lower bound and the reversals x_{i+1} are limited by the additive noise term η_i. There is also an upper bound and x_{i+1} are limited by the contrast modulation and the frame interleaving of the color monitor [67]. The ratio $\rho = (F_\eta/F_\lambda)^{1/2}$ defines the balance between the multiplicative and the additive noise strength in Eqs. (4) and (5) and for small additive noise ($0 < \rho < 1$) [91] and consequently in color vision the additive term $\langle \eta_i \rangle$ is near zero. To evaluate the ratio ρ, we have simplified the situation and have assumed that $\omega + \varepsilon \cong 2$ and $(J_\eta/J_\lambda) \cong 1 + (T_F/S_F)$, where T_F and S_F are the temporal and the spatial frequency of achromatic stimuli [67–69] and for the ratio $\rho \cong C(1 + T_F/S_F)^{1/2}$. For red-green isoluminant stimuli the dependency on T_F and S_F is not considered [67] and the ratio is just the mask contrast $\rho = C$.

It has been demonstrated that the moments m_r of the stationary PDF in the Langevin model will approach a power function as a function of ρ in the limit $\rho \to 0$, i.e., for vanishing strength of the additive noise with respect to the multiplicative noise term [91]:

$$\langle m_r \rangle \cong G_0 + G_1 \rho^{H(r)}, \tag{6}$$

where G_0 and G_1 are constant values. The exponent $H(r)$ depends on the scaling exponent of the power law of the PDF as well as the order of moments r [91]. Taking the mean $\mu \equiv \langle m_1 \rangle = G_0 + G_1 \rho^{H(1)}$ and the second-order moment centered around the mean $\sigma^2 \equiv \langle m_2 \rangle = G_0{}' + G_1{}' \rho^{H(2)}$, and assuming that G_0 and $G_0{}'$ are small values in m_1 and m_2, respectively, fluctuation scaling in Eq. (1) is derived as follows:

$$\sigma^2 \cong \frac{G_1{}'}{G_1{}^{H(2)/H(1)}} \mu^{H(2)/H(1)}. \tag{7}$$

Therefore, the scaling exponent β in Eq. (1) and the exponent $H(r)$ in Eq. (6) are related, $\beta = H(2)/H(1)$. Furthermore, we consider the third- and fourth-order moments centered around the mean by $\langle m_3 \rangle = G_0{}'' + G_1{}'' \rho^{H(3)}$ and $\langle m_4 \rangle = G_0{}''' + G_1{}''' \rho^{H(4)}$, respectively, and assuming that $G_0{}'' \cong 0$ [91], the same reasoning in Eq. (7) holds for the S-K relation. By using $\langle m_3 \rangle = S_0 m_2^{3/2}$ and $\langle m_4 \rangle = K_0 m_2^2$, it follows for the S-K relation that

$$\begin{aligned} K_0 &\cong A S_0{}^{H(4)/H(3)} + B, \\ A &= \left(\frac{G_1{}'''}{G_1{}''^{1/H(3)}} \right) m_2{}^{[3H(4)/2H(3)]-2}, \\ B &= \left(\frac{G_0{}'''}{m_2^2} \right). \end{aligned} \tag{8}$$

We examine two special cases:

(i) If $H(r) = r$ [91] and $B \cong 0$, Eq. (8) will approach the 4/3 power function regime:

$$\begin{aligned} K_0 &\cong A S_0{}^{4/3}, \\ A &= \left(\frac{G_1{}'''}{G_1{}''^{1/3}} \right). \end{aligned} \tag{9}$$

(ii) If $H(4)/H(3) = 2$ and $B \neq 0$, Eq. (8) will recover the quadratic relation in Eq. (3):

$$\begin{aligned} K_0 &\cong A S_0{}^2 + B, \\ A &= m_2 \left(\frac{G_1{}'''}{G_1{}''^{1/H(3)}} \right), \\ B &= \left(\frac{G_0{}'''}{m_2^2} \right). \end{aligned} \tag{10}$$

Figure 6 represents in a double logarithmic plot the mean μ, the variance σ^2, the absolute value of third-order moment $|m_3| = |S_1 \sigma^3|$, and the fourth-order moment $m_4 = K_1 \sigma^4$ as a function of $\rho \cong C(1 + T_F/S_F)^{1/2}$.

Figure 6 demonstrates that all the moments increase as ρ increases as expected from Eq. (6) in the limit of weak additive noise although there is some broadening. We have examined the exponents of Eqs. (7) and (8). A linear least-squares regression was performed for each case in a log-log plot (Fig. 6). The scaling exponent $H(r)$ for μ, σ^2, $|m_3|$, and m_4 was $H(1) = 0.35$, $H(2) = 0.83$, $H(3) = 1.13$, and $H(4) = 1.7$, respectively, and the 95% confidence interval was $H(1) \in (0.32, 0.38)$, $H(2) \in (0.73, 0.93)$, $H(3) \in (0.97, 1.30)$, and $H(4) \in (1.44, 1.89)$, respectively. The goodness-of-fit indicates that in all cases ($0.41 < R^2 < 0.63$). However, from Eq. (7) the ratio of the scaling exponents leads to $H(2)/H(1) = 2.32$, which is a very good approximation to the scaling exponent of fluctuation scaling in Eq. (1), $\beta = 2.48$ [Fig. 4(a)]. From Eq. (8), the ratio of the scaling exponents leads to $H(4)/H(3) = 1.5$. This is a reasonable approximation to the quadratic polynomial in Eq. (3) [Fig. 4(b)]. Taking the ratio of the upper to the lower 95% confidence intervals, $H(4)/H(3) \cong 1.89/0.97 = 1.94$, which is very close to the exponent of the quadratic relation in Eq. (3).

F. Discussion

Many studies in sensory psychophysics often assume that trial-to-trial and day-to-day threshold variability is an unpredictable residual fluctuation that does not exhibit correlation across conditions. However, Fig. 4(a) clearly shows that

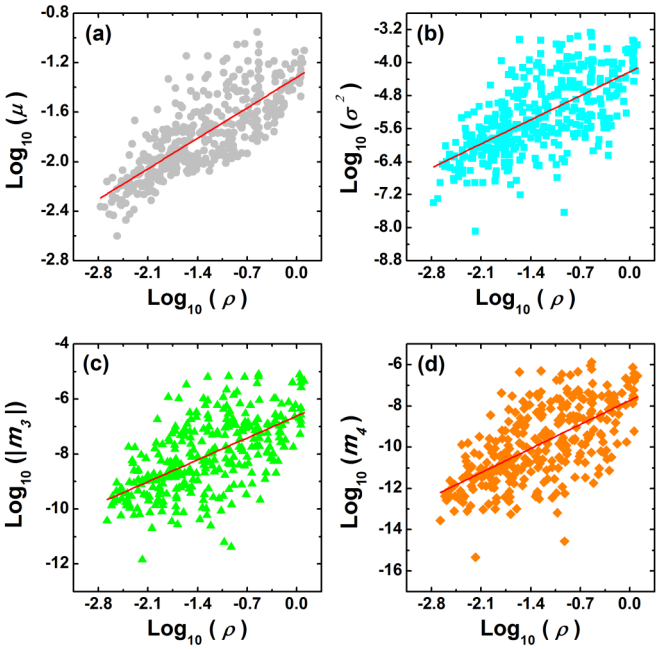

FIG. 6. Double logarithmic plot ($\log_{10}$) of the first four moments m_r as a function of the strength of the additive noise ρ. (a) Mean μ. (b) Variance σ^2. (c) Absolute value of the third moment m_3. (d) Fourth moment m_4. In each panel the solid line corresponds to a linear regression analysis. The corresponding slopes ($\pm$ standard error) for μ, σ^2, $|m_3|$, and m_4 are 0.35 ± 0.01, 0.83 ± 0.05, 1.13 ± 0.08, and 1.7 ± 0.1, respectively.

threshold variability is correlated over multiple trials for a wide range of spatial and temporal frequencies, mask contrast values, viewing conditions (binocular and monocular), type of stimuli (achromatic and red-green isoluminant), and masking effects (threshold elevation and facilitation). The sample variance σ^2 scales with the sample mean μ and obeys a power function averaged across subjects. A broadening is observed in Figs. 4 and 6 as in many other studies of fluctuation scaling [7,10,12,18,19,24,56]. Broadening effects in human psychophysics are the result of many causes. They may include different experimental factors that are difficult to control, such as interindividual differences, fatigue, inattention, etc. Although 2AFC staircase processes are standard and minimize response bias, another possible cause of observed broadening is that 2AFC staircases are contaminated by the effects of interval and sample bias [34,81]. In general, broadening produces poor fits [7] and corrections to fluctuations scaling but a unified theoretical approach remains unresolved [7]. Nonetheless fluctuation scaling between σ^2 and μ in Fig. 4(a) is not an artifact from the effects of bias but it truly represents a coarsely grained effect that explains most of the total percent of variability of data points (74.6%). Figure 4(a) also demonstrates that threshold variability for both achromatic and red-green isoluminant stimuli is modeled by the power function in Eq. (1) with a scaling exponent different from 2 ($\beta = 2.48 \pm 0.07$). This implies that fluctuation scaling is supported by different post-receptoral parallel visual pathways that process achromatic and red-green isoluminant stimuli [78,94].

We also demonstrate that the skewness S and the kurtosis K of thresholds are clustered in a U-shaped pattern. The quadratic relationship in Eq. (3) fit the data remarkably well over a wide range of masking conditions [Fig. 4(b)]. The quadratic model is a robust result and indicates that the PDFs at all mask conditions are related between them and can be described by a few classes of non-Gaussian PDFs [36,38,42,51,55]. The results in Fig. 4(b) indicate that the scaling exponent is 2 and departs from the 4/3 power function regime [16], in the same way as many complex systems [36–43,45–50].

Previous works have found that very large values in the S-K plane are better described by the 4/3 power function in the distribution of earthquakes, financial data, etc. [56,58]. These results were analyzed by dividing very large datasets into subsamples of a certain fixed length. S and K values were calculated for each subsample window [56,58]. Our threshold data were not analyzed in the same way as in [56,58]. Here the skewness S and the kurtosis K of threshold distributions were calculated at the reversal points for each stimulus condition separately and the number of staircase sessions in each condition was not fixed but variable (see Sec. III). A finite number of data points could be the reason that the tails of threshold distributions can be sampled incompletely [58] and thus, the absence of very large K and S values outside from the parabolic region [56,58]. Finite-size effects from limited sampling could have some influence in the coefficients A and B of Eq. (3) and in the goodness-of-fit by clustering data points slightly different in the S-K plane [Fig. 4(b)]. However, in our psychophysical experiments very large threshold variability as a function of the trial number is not usually observed under well-controlled conditions in the laboratory such as in 2AFC staircases. The amplitude of the reversals is small and the reversals are always bounded ($0 < x_{i+1} < 1$) (Fig. 2). Therefore, extreme deviations are not expected from one experimental session to another, etc. That is why very large K and S values derived from extreme events are not observed in Fig. 4(b) and consequently, our threshold data do not approximate to the 4/3 power function regime as well.

The remarkable similarity of fluctuations in the S-K plane between many different fields has led several authors to conjecture that the universal character of Eq. (3) and the nature of non-Gaussian PDFs could arise from common basic features [55,60,62,63]. It is often assumed that K and S depend on a few control parameters ζ_i $[K(\zeta_i), S(\zeta_i)]$, and equivalently in Eq. (3), $K = A(\zeta_i)S^2 + B(\zeta_i)$ [38,43,49,59,60,62]. In plasma physics, fluctuations are mainly generated by the internal dynamics although external driving, such as in magnetized plasmas, also plays a functional role in plasma turbulence [43]. Different approaches have included intermittent dynamics, blob structures, burstlike patterns, and coherent structures and additive noise [43,55,60,62,63]. In climate variability, fluctuations are mainly modulated by external sources which act in a similar way as cross-orientation masking. A Langevin equation with multiplicative and weak additive noise has been presented to describe plasma turbulence [38,42,59] and fluctuations in many variables in the ocean and in the atmosphere [38]. This model also predicts the existence of power laws in the right tails of PDFs [38]. Although this Langevin approach is in agreement with the experimental

values of the coefficient A, their approach is limited because it is assumed that B is an empirical constant for any experiment [38,42,59]. Furthermore, in certain situations, such as in contaminant concentration fluctuations in the atmosphere, the coefficients A and B do not have to be necessarily independent [49]. In general, A and B values are in a range 1–7 for a wide set of physical processes [36–50] including human color vision [Fig. 4(b)].

In sensory psychophysics, we found that intermittency is a fundamental feature of time series in 2AFC processes. A stochastic process driven by both random multiplicative and weak additive noise is proposed based on a similar Lanvegin-type equation. In a previous study, the mechanisms that lead to asymptotic power law of moments [Eq. (6)] and power-law behavior of PDFs were clarified [91]. However, the unification between fluctuation scaling in Eq. (1) and the quadratic relation in Eq. (3) was not investigated. Here we have adapted and extended the Langevin model proposed in [91] to provide a unifying framework within the context of human color vision. Our approach is different from the Langevin model used in climate and plasma physics [38,42,59], in the sense that the weak additive noise term has an unexpected role in cross-orientation masking. The weak additive noise is signal dependent and has a significant effect in the shape of the TvC functions by promoting a threshold elevation at high mask contrasts [Fig. 5]. The weak additive noise also governs the moments of the PDF of thresholds (Fig. 6) [91]. Our Langevin approach unifies fluctuation scaling together with the quadratic relation and the $4/3$ power function in the S-K plane. Our Langevin model also provides a meaning to the empirical coefficients α and β and A and B in Eqs. (1) and (3), respectively. It clarifies the main features of the TvC functions and the dipper effect (Fig. 5), and predicts the scaling exponents of fluctuation scaling and the S-K quadratic relation in human color vision [see Eqs. (7)–(10) and Fig. 6]. Because the Langevin model developed in [91] is quite general and does not depend on the details of boundary conditions and the nature of the noise terms, the theoretical results in Eqs. (7)–(10) may contribute to develop approaches that seek to understand fluctuation scaling and on-off intermittency under external stimulus driving in neurophysiology, econophysics, atmospheric and plasma turbulence, etc.

V. CONCLUDING REMARKS

We have investigated the non-Gaussian properties of contrast detection threshold distributions for plaid patterns or cross-orientation masking. We have used the mean, the variance, the skewness, and the kurtosis measured at the reversal points of time series in a 2AFC staircase process. We demonstrate that contrast thresholds are governed by on-off intermittency (Fig. 2) and follow fluctuation scaling with a nonuniversal scaling exponent ($\beta = 2.48 \pm 0.07$) over a wide range of experimental conditions [Fig. 4(a)]. We also find that the shape of threshold distributions is related between stimulus conditions and can be described by a unique quadratic relation in the skewness-kurtosis plane $K_1 = (1.19 \pm 0.04)S_1^2 + (2.68 \pm 0.06)$ [Fig. 4(b)]. The quadratic relation departs from the $4/3$ power function of the generalized version of fluctuation scaling. This quadratic relation has a powerful impact in the statistical properties of threshold distributions and shares common organizing principles with plasma physics and climate variability, etc. A random multiplicative process with weak additive noise provides a unifying description of fluctuation scaling and the S-K relations; it predicts the corresponding scaling exponents (Fig. 6) as well as the shape of the TvC functions (Fig. 5). Our findings are of importance for better understanding the functional role of intermittency in sensory perception and could be relevant for designing better brain-machine interfaces.

ACKNOWLEDGMENTS

We thank all the participants of this study for their support and effort.

[1] C. M. Harris and D. M. Wolpert, Nature (London) **394**, 780 (1998).
[2] R. B. Stein, E. R. Gossen, and K. E. Jones, Nat. Rev. Neurosci. **6**, 389 (2005).
[3] S. W. S. MacDonald, L. Nyberg, and L. Bäckman, Trends Neurosci. **29**, 474 (2006).
[4] G. Deco and R. Romo, Trends Neurosci. **31**, 591 (2008).
[5] A. A. Faisal, L. P. J. Selen, and D. M. Wolpert, Nat. Rev. Neurosci. **9**, 292 (2008).
[6] C. T. Kello, G. D. A. Brown, R. Ferrer-i-Cancho, J. G. Holden, K. Linkenkaer-Hansen, T. Rhodes, and G. C. Van Orden, Trends Cogn. Sci. **14**, 223 (2010).
[7] Z. Eisler, I. Bartos, and J. Kertész, Adv. Phys. **57**, 89 (2008).
[8] Z. Eisler and J. Kertész, Phys. Rev. E **73**, 046109 (2006).
[9] L. R. Taylor, Nature (London) **189**, 732 (1961).
[10] W. S. Kendal, Ecol. Complex. **1**, 193 (2004).
[11] B. J. West, Front. Physiol. **1**, 12 (2010).
[12] A. Fronczak and P. Fronczak, Phys. Rev. E **81**, 066112 (2010).
[13] W. S. Kendal and B. Jørgensen, Phys. Rev. E **84**, 066120 (2011).
[14] W. S. Kendal and B. Jørgensen, Phys. Rev. E **83**, 066115 (2011).
[15] W. S. Kendal, Physica A **421**, 141 (2015).
[16] A. Giometto, M. Formentin, A. Rinaldo, J. E. Cohen, and A. Maritan, Proc. Natl. Acad. Sci. USA **112**, 7755 (2015).
[17] J. E. Cohen and M. Xu, Proc. Natl. Acad. Sci. USA **112**, 7749 (2015).
[18] J. P. Onnela and F. Reed-Tsochas, Proc. Natl. Acad. Sci. USA **107**, 18375 (2010).
[19] Y. Wang, Q. Zhang, C. Zhu, M. Hu, and V. Duong, Physica A **441**, 151 (2016).
[20] D. J. Tolhurst, J. A. Movshon, and A. F. Dean, Vision Res. **23**, 775 (1983).
[21] M. Carandini, PLoS. Biol. **2**, e264 (2004).
[22] M. M. Churchland *et al.*, Nat. Neurosci. **13**, 369 (2010).
[23] S. Sadagopan and D. Ferster, Neuron **74**, 911 (2012).
[24] D. Moshitch and I. Nelken, J. Neurosci. Meth. **225**, 13 (2014).
[25] S. Koyama, Neural Comput. **27**, 1530 (2015).

[26] J. A. Swets, W. P. Tanner, Jr., and T. G. Birdsall, Psychol. Rev. **68**, 301 (1961).
[27] R. D. Luce, *Response Times* (Oxford University Press, New York, 1986), p. 562.
[28] J. A. Solomon, Vision Res. **47**, 3247 (2007).
[29] E. J. Wagenmakers and S. Brown, Psychol. Rev. **114**, 830 (2007).
[30] F. Schmiedek, M. Lövdén, and U. Lindenberger, Psychol. Aging **24**, 841 (2009).
[31] X. Xiao, E. P. White, M. B. Hooten, and S. L. Durham, Ecology **92**, 1887 (2011).
[32] M. P. H. Stumpf and M. A. Porter, Science **335**, 665 (2012).
[33] G. A. Gescheider, *Psychophysics: The Fundamentals* (Taylor & Francis, London, 1997).
[34] S. A. Klein, Percept. Psychophys. **63**, 1421 (2001).
[35] H. Cramér, *Mathematical Methods of Statistics* (Princeton University Press, Princeton, NJ, 1945).
[36] B. Labit, I. Furno, A. Fasoli, A. Diallo, S. H. Müller, G. Plyushchev, M. Podestà, and F. M. Poli, Phys. Rev. Lett. **98**, 255002 (2007).
[37] J. Cheng *et al.*, Plasma Phys. Contr. F. **52**, 055003 (2010).
[38] P. Sura, Atmos. Res. **101**, 1 (2011).
[39] H. Zushi, N. Nishino, K. Hanada, H. Honma, H. Q. Liu, Y. Higashizono, M. Sakamoto, S. Tashima, and T. Ryoukai, J. Nucl. Mater. **415**, S624 (2011).
[40] D. L. Toufen, Z. O. Guimarães-Filho, I. L. Caldas, J. D. Szezech, S. R. Lopes, R. L. Viana, and K. W. Gentle, Phys. Plasmas **20**, 022310 (2013).
[41] H. Q. Liu *et al.*, J. Nucl. Mater. **438**, S513 (2013).
[42] S. Banerjee *et al.*, Phys. Plasmas **21**, 072311 (2014).
[43] A. S. Bergsaker, F. Å, H. L. Pécseli, and J. K. Trulsen, Phys. Scr. **90**, 108005 (2015).
[44] H. Mezaoui, A. M. Hamza, and P. T. Jayachandran, Geo. Phys. Res. Lett. **41**, 6570 (2014).
[45] N. Mole and E. D. Clarke, Bound.-Layer Meteorol. **73**, 35 (1995).
[46] P. C. Chatwin and C. Robinson, Nuovo Cimento C **20**, 361 (1997).
[47] D. M. Lewis and P. C. Chatwin, J. Appl. Meteorol. **36**, 1064 (1997).
[48] S. Alberghi, A. Maurizi, and F. Tampieri, J. Appl. Meteorol. **41**, 885 (2002).
[49] T. P. Schopflocher and P. J. Sullivan, Bound.-Layer Meteorol. **115**, 341 (2005).
[50] K. E. Chlouverakis, S. Mikroulis, and D. Syvridis, in *Semiconductor Lasers and Laser Dynamics III*, edited by K. P. Panajotov *et al.* (Proceedings of SPIE, Strasbourg, 2008), pp. 699–717.
[51] D. L. Ringach and B. J. Malone, J. Neurosci. **27**, 7673 (2007).
[52] K. Pearson, Philos. Trans. R. Soc. London Sect. A **216**, 429 (1916).
[53] J. E. Wilkins, Ann. Math. Stat. **15**, 333 (1944).
[54] C. A. J. Klaassen, P. J. Mokveld, and B. van Es, Stat. Probabil. Lett. **50**, 131 (2000).
[55] F. Sattin, M. Agostini, R. Cavazzana, G. Serianni, P. Scarin, and N. Vianello, Phys. Scr. **79**, 045006 (2009).
[56] M. Cristelli, A. Zaccaria, and L. Pietronero, Phys. Rev. E **85**, 066108 (2012).
[57] S. C. Kerman and J. B. McDonald, Stat. Probabil. Lett. **83**, 2129 (2013).
[58] A. Celikoglu and U. Tirnakli, Phys. Rev. E **92**, 066801 (2015).
[59] J. A. Krommes, Phys. Plasmas **15**, 030703 (2008).
[60] I. Sandberg, S. Benkadda, X. Garbet, G. Ropokis, K. Hizanidis, and D. del-Castillo-Negrete, Phys. Rev. Lett. **103**, 165001 (2009).
[61] H. E. Jørgensen, T. Mikkelsen, and H. L. Pécseli, Bound.-Layer Meteorol. **137**, 345 (2010).
[62] D. Guszejnov, N. Lazányi, A. Bencze, and S. Zoletnik, Phys. Plasmas **20**, 112305 (2013).
[63] P. P. Galuzio, S. R. Lopes, G. Z. dos Santos Lima, R. L. Viana, and M. S. Benkadda, Physica A **402**, 8 (2014).
[64] D. N. Joanes and C. A. Gill, J. R. Stat. Soc. D **47**, 183 (1998).
[65] D. H. Hubel and T. N. Wiesel, J. Physiol. London **195**, 215 (1968).
[66] J. M. Foley, J. Opt. Soc. Am. A **11**, 1710 (1994).
[67] J. M. Medina and K. T. Mullen, J. Vision **9**, 20 (2009).
[68] T. S. Meese and D. J. Holmes, Proc. R. Soc. B Biol. Sci. **274**, 127 (2007).
[69] J. M. Medina, J. Carvalho, and S. Franco, in *33rd European Conference on Visual Perception*, edited by T. Meese, P. Thompson, and T. Troscianko (Perception 39 supplement, Lausanne, 2010), pp. 203.
[70] M. C. Morrone, D. C. Burr, and L. Maffei, Proc. R. Soc. B Biol. Sci. **216**, 335 (1982).
[71] A. B. Bonds, Visual Neurosci. **2**, 41 (1989).
[72] N. J. Priebe and D. Ferster, Neuron **75**, 194 (2012).
[73] M. Carandini, and D. J. Heeger, Nat. Rev. Neurosci. **13**, 51 (2012).
[74] J. M. Medina, J. Carvalho, and S. Franco, in *21st International Conference on Noise and Fluctuations*, edited by M. J. Deen and C. H. Chen (IEEE Conference Proceedings, Toronto, 2011), pp. 421.
[75] D. G. Pelli, Spat. Vis. **10**, 437 (1997).
[76] D. H. Brainard, Spat. Vis. **10**, 433 (1997).
[77] V. S. Graham, *Visual Pattern Analyzers* (Oxford University Press, New York, 1989).
[78] S. G. Solomon and P. Lennie, Nat. Rev. Neurosci. **8**, 276 (2007).
[79] G. R. Cole, T. Hine, and W. McIlhagga, J. Opt. Soc. Am. A **10**, 38 (1993).
[80] V. C. Smith and J. Pokorny, Vision Res. **15**, 161 (1975).
[81] M. A. García-Pérez, Vision Res. **38**, 1861 (1998).
[82] W. Press, S. Teukolsky, W. Vetterling, and B. Flannery, *Numerical Recipes in C* (Cambridge University Press, Cambridge, 1992).
[83] T. S. Meese, K. L. Challinor, and R. J. Summers, Visual Neurosci. **25**, 585 (2008).
[84] F. Moss, L. M. Ward, and W. G. Sannita, Clin. Neurophysiol. **115**, 267 (2004).
[85] J. v. Neumann, R. H. Kent, H. R. Bellinson, and B. I. Hart, Ann. Math. Stat. **12**, 153 (1941).
[86] N. Platt, S. M. Hammel, and J. F. Heagy, Phys. Rev. Lett. **72**, 3498 (1994).
[87] J. F. Heagy, N. Platt, and S. M. Hammel, Phys. Rev. E **49**, 1140 (1994).
[88] N. Platt, E. A. Spiegel, and C. Tresser, Phys. Rev. Lett. **70**, 279 (1993).
[89] J. L. Cabrera and J. G. Milton, Phys. Rev. Lett. **89**, 158702 (2002).

[90] A. Hramov, A. A. Koronovskii, I. S. Midzyanovskaya, E. Sitnikova, and C. M. van Rijn, Chaos **16**, 043111 (2006).
[91] H. Nakao, Phys. Rev. E **58**, 1591 (1998).
[92] W. T. Coffey, Y. P. Kalmykov, and J. T. Waldron, *The Langevin Equation* (World Scientific, Singapore, 2004), p. 678.
[93] G. A. Cecchi, M. Sigman, J. M. Alonso, L. Martinez, D. R. Chialvo, and M. O. Magnasco, Proc. Natl. Acad. Sci. USA **97**, 5557 (2000).
[94] P. Lennie and J. A. Movshon, J. Opt. Soc. Am. A **22**, 2013 (2005).
[95] D. Sornette and R. Cont, J. Phys. I France **7**, 431 (1997).
[96] H. Takayasu, A. H. Sato, and M. Takayasu, Phys. Rev. Lett. **79**, 966 (1997).
[97] D. Sornette, Phys. Rev. E **57**, 4811 (1998).
[98] J. M. Medina, Phys. Lett. A **376**, 1617 (2012).